Dalton Transactions

Accepted Manuscript

This is an *Accepted Manuscript*, which has been through the Royal Society of Chemistry peer review process and has been accepted for publication.

Accepted Manuscripts are published online shortly after acceptance, before technical editing, formatting and proof reading. Using this free service, authors can make their results available to the community, in citable form, before we publish the edited article. We will replace this *Accepted Manuscript* with the edited and formatted *Advance Article* as soon as it is available.

You can find more information about *Accepted Manuscripts* in the Information for Authors.

Please note that technical editing may introduce minor changes to the text and/or graphics, which may alter content. The journal's standard Terms & Conditions and the Ethical guidelines still apply. In no event shall the Royal Society of Chemistry be held responsible for any errors or omissions in this *Accepted Manuscript* or any consequences arising from the use of any information it contains.

ROYAL SOCIETY OF CHEMISTRY

www.rsc.org/dalton

Journal Name

ARTICLE

Thermal Degradation Mechanism of Triangular Ag@SiO_2 Nanoparticles

Received 00th January 20xx,
Accepted 00th January 20xx

DOI: 10.1039/x0xx00000x

www.rsc.org/

Mahesh K. Gangishetty, Robert W. J. Scott*, Timothy L. Kelly*

Triangular silver nanoparticles are promising materials for light harvesting applications because of their strong plasmon bands; these absorption bands are highly tunable, and can be varied over the entire visible range based on the particle size. A general concern with these materials is that they are unstable at elevated temperatures. When thermally annealed, they suffer from changes to the particle morphology, which in turn affects their optical properties. Because of this stability issue, these materials cannot be used in applications requiring elevated temperatures. In order to address this problem, it is important to first understand the degradation mechanism. Here, we measure the changes in particle morphology, oxidation state, and coordination enviornment of Ag@SiO_2 nanotriangles caused by thermal annealing. UV-vis spectroscopy and TEM reveal that upon annealing the Ag@SiO_2 nanotriangles in air, the triangular cores are truncated and smaller nanoparticles are formed. Ag *K*-edge X-ray absorption spectroscopy (XANES and EXAFS) shows that the small particles consist of Ag(0), and that there is a decrease in the Ag-Ag coordination number with an increase in the annealing temeperature. We hypothesize that upon annealing Ag in air, it is first oxidized to Ag_xO, after which it subsequently decomposes back to well-dispersed Ag(0) nanoparticles. In contrast, when the Ag@SiO_2 nanotriangles are annealed in N_2, since there is no possibility of oxidation, no small particles are formed. Instead, the triangular core rearranges to form a disc-like shape.

Introduction

Localized surface plasmon resonance (LSPR) is a phenomenon unique to metal nanoparticles, and has a wide variety of applications. When metal nanoparticles interact with incoming light, the light drives coherent oscillations of the electrons in their conduction bands, known as localized surface plasmons. LSPR occurs when the frequency of these oscillations is in resonance with the frequency of the incoming light.[1-3] Due to their unique optical properties, they have been used in a variety of applications such as surface-enhanced Raman spectroscopy,[4, 5] sensing,[6-8] photocatalysis[9-14] and optoelectronics.[15-19] The frequency of the LSPR band depends on both the type of material (e.g., Au, Ag or Cu), and the shape and size of the nanoparticles.[1, 4]

Triangular Ag nanoparticles have high extinction coefficients and their optical properties are easily tunable by changing the edge length.[20] In addition to this, they exhibit very intense near fields as the charge that arises from the plasmon oscillations is concentrated near the tips. Because of this strong LSPR and the corresponding strong near field effects, they have been efficient materials for light harvesting applications.[15, 21-23] However, a major concern with these materials is their stability.[24] There have been numerous studies, both theoretical and experimental, on the stability of Ag nanotriangles. Any oxidation promoting reagents such as halide ions[24, 25] and thiols[26] attack the tips of the triangles, causing a change in particle morphology which affects their optical properties. In addition to these chemical reagents, UV irradiation[27, 28] and heating the colloidal solutions[28-30] also have detrimental effects on the morphology of these triangles. All of the above treatments degrade the tips of the triangle, and similar behaviour is observed for other particles with sharp features, such as nanowires,[30, 31] tetrahedra,[32] and nanocubes.[33] To protect them from chemical etching agents, such particles are often coated with different materials such as SiO_2,[15, 34] TiO_2[35] and Au.[23, 24, 36] However, protecting the nanotriangles from thermal degradation is quite challenging, and the presence of porous SiO_2 or TiO_2 shells may not be enough to prevent decomposition. Lei *et al.* observed the degradation of Ag nanospheres at elevated temperatures even after coating with a thin silica shell, as oxygen from the atmosphere diffused through the porous silica and led to the oxidation of the Ag core.[37]

The stability of nanoparticles depends on their surface energy. Ag has a face centered cubic crystal structure, and the triangular nanoparticles are enclosed by low energy (111) planes on their basal surfaces and high energy (110) or (100) planes on their edges.[30] The surface energies of these crystal planes follow the order (100) > (110) > (111).[38] As per the Gibbs-

*Address correspondence to: tim.kelly@usask.ca and robert.scott@usask.ca. Department of Chemistry, University of Saskatchewan, 110 Science Place, Saskatoon, SK, S7N 5C9, Canada

Electronic Supplementary Information (ESI) available: UV-vis spectrum and TEM image of Ag@SiO_2 nanotriangles, and TEM images of SiO_2@Ag samples after annealing. See DOI: 10.1039/x0xx00000x

Dalton Transactions Accepted Manuscript

Please do not adjust margins

Thomson effect, the tips are even more unstable than the edges, since they are formed by the intersection of two high energy facets (the edges). Hence, the decomposition of these particles begins with the dissociation of atoms from the tips, followed by the edges.[39] The dissociated atoms are either redeposited on the more stable basal planes, leading to the formation of thick nanodiscs, or they completely detach from the nanoparticle resulting in a reduction in the overall particle size.[29, 39] Tang *et al*. observed dissociation of Ag atoms from the tips of triangles and the formation of circular nanodiscs upon aging Ag nanotriangles at 95 °C.[29] Upon irradiating the solution of degraded Ag nanotriangles with a sodium lamp, reconstruction to the original morphology of nanotriangles was observed.[28] Many groups have similarly used mild heating in solvent as a route for synthesizing Ag circular nanodiscs from triangular precursors.[29, 40] Although it is clear that the Ag nanotriangles are forming circular nanodiscs upon decomposition, there are several questions that are left unaddressed about the mechanism of degradation. It has been noted that the overall size of the nanoparticles decreases upon annealing at elevated temperatures,[24, 29] where the fate of the dissociated atoms needs to be fully understood.

Here, we elucidate the mechanism of thermal degradation of Ag@SiO_2 nanotriangles by using X-ray absorption spectroscopy (XAS). XAS is a powerful tool for understanding changes in oxidation state, atomic environment and first shell coordination number (and thus average particle size) during the shape transformation of the nanotriangles. We synthesized the Ag@SiO_2 nanotriangles and annealed them in both air and N_2 atmospheres at different temperatures, ranging from 150 °C to 600 °C. The Ag *K*-edge spectra were recorded for all samples before and after annealing. Our analysis showed that upon annealing the Ag@SiO_2 nanotriangles in air, the Ag core breaks up to form multiple smaller Ag particles. We hypothesize that the Ag core is first oxidized to Ag_xO, which then further dissociates to form small Ag nanoparticles in the pores of the silica spheres. Further evidence for this mechanism is found by studying samples annealed in N_2, which do not show such formation of small Ag nanoparticles.

Experimental

Materials and methods

Silver nitrate (99%), sodium borohydride (98%), and hydrogen peroxide (30% w/w), were purchased from Fisher Scientific. Trisodium citrate dihydrate (≥ 96%), poly (*N*-vinylpyrrolidone) (PVP, ≥ 99%, MW 40,000 g/mol), 16-mercaptohexadecanoic acid (MHA, 90%), tetraethoxysilane (TEOS, 99%), and *N*,*N*-dimethylamine (40% w/v) were purchased from Sigma-Aldrich. All chemicals were used as received without further purification. Deionized water (18.2 MΩ·cm) was obtained from a Milli-Q water purification system.

Synthesis of Ag and Ag@SiO_2 nanotriangles

Triangular Ag and Ag@SiO_2 nanoparticles were synthesized by using existing procedures.[15, 41] To 248 mL of deionized water, aqueous solutions of $AgNO_3$ (500 µL, 50 mM), trisodium citrate (5 mL, 75 mM), PVP (1 mL, 17.5 mM) and H_2O_2 (600 µL) were added. Finally, aqueous $NaBH_4$ (2.5 mL, 0.1 M) was rapidly injected into the solution. After the formation of a blue coloured solution, the nanotriangles were collected by centrifugation (10,000 g, 3.5 h).

After centrifugation, the nanotriangles were dispersed in 100 mL deionized water, followed by the addition of an ethanolic MHA solution (1.5 mL, 5 mM) and stirring for 10 min. The MHA-functionalized Ag nanotriangles were centrifuged (10,000 g, 3.5h) and redispersed in ethanolic TEOS (20 mL, 16 mM). After 2 min of stirring, aqueous dimethylamine (2 mL, 20% w/v) was added and the solution was stirred for 12 h. The Ag@SiO_2 nanotriangles were collected by centrifugation (10,000 g, 1 h) and dried at room temperature. To prepare the SiO_2@Ag control samples (triangular Ag nanoparticles adsorbed on SiO_2 spheres), first SiO_2 nanospheres were synthesized by stirring a mixture of TEOS and dimethylamine (using the same concentrations as above) for 12 h in ethanol. After purifying the SiO_2 nanoparticles by centrifugation and redispersion, an aqueous solution of MHA-functionalized Ag nanotriangles was added and stirred for 2 h. The SiO_2@Ag sample was then isolated by centrifugation.

Thermal annealing studies

To study the thermal degradation of the Ag@SiO_2 nanotriangles, they were annealed at different temperatures (150 °C, 300 °C, 450 °C and 600 °C) in either an air or N_2 atmosphere. The samples were heated at a rate of 10 °C/min and the dwell time at the final temperature was 15 min. A Lindberg/Blue M tube furnace was used to carry out the annealing studies, and a flow of N_2 was used to generate the N_2 atmosphere.

Characterization

Transmission electron microscopy (TEM) images were collected using a Hitachi HT7700 TEM operating at 100 kV. TEM samples were prepared by drop casting the nanoparticle solution onto a carbon-coated 300 mesh Cu TEM grid.

UV–visspectra were measured using a Varian Cary 50 Bio UV–vis spectrophotometer with an optical path length of 1 cm.

X-ray absorption measurements were performed at the Hard X-ray MicroAnalysis (HXMA) beamline 061D-1 (energy range 5–40 keV; resolution, 1×10^{-4} ΔE/E) at the Canadian Light Source (CLS, 2.9 GeV storage ring, 250 mA current). A double-crystal Si monochromator was used for energy selection of the Ag *K*-edge (25514 eV). All samples were in the form of solid powders and were mixed with boron nitride (to give a 5% w/w Ag loading) and then pelletized before analysis. Measurements were taken in both transmission and fluorescence mode concurrently. The data analysis and extended X-ray Absorption Fine Structure (EXAFS) fitting were performed by using the IFEFFIT software package.[42, 43] We used Ag (Fm-3m) crystallographic data to fit the Ag-foil spectrum. First, fitting was performed on the Ag-foil spectrum, keeping the coordination number fixed (CN = 12) in order to determine the amplitude

Dalton Transactions Accepted Manuscript

This journal is © The Royal Society of Chemistry 20xx

reduction factor (S_o^2). From this fitting, the amplitude reduction factor determined for the Ag-foil was 0.973 and was used for the subsequent sample fits.

Results and discussion

Ag@SiO_2 nanotriangles were first synthesized by following previously published procedures.[15] Briefly, the Ag nanotriangles were synthesized by reducing $AgNO_3$ using $NaBH_4$ in the presence of trisodium citrate and H_2O_2. Subsequently, these nanotriangles were functionalized with 16-mercaptohexadecanoic acid. These functionalized Ag nanotriangles were then used to prepare the Ag@SiO_2 core@shell nanotriangles using a Stöber sol-gel process. The nanoparticles were then characterized by UV-vis spectroscopy and transition electron microscopy. Fig. S1a shows the UV-vis spectra of the MHA-functionalized and Ag@SiO_2 nanotriangles. The peak at 725 nm, the shoulder at 490 nm, and the peak at 330 nm can be ascribed to the in-plane dipole, in-plane quadrupole, and the out-of-plane quadrupole plasmon modes, respectively. TEM images were recorded for these samples, and are shown in Fig. S1b. TEM shows the presence of a ~ 30 nm thick silica shell around the Ag nanotriangles.

Thermal degradation study of Ag@SiO_2 using UV-vis and TEM

After synthesizing the Ag@SiO_2 nanotriangles, they were subjected to different annealing temperatures in order to understand their thermal stability. The annealing temperatures were varied from 150 °C to 600 °C, and the annealing was done in both air and N_2 atmospheres. After annealing, the samples were redispersed in ethanol by sonication, characterized by UV-vis and TEM, and compared with the samples before annealing. Fig. 1 shows the normalized UV-vis spectra of the Ag@SiO_2 samples before and after annealing in air (Fig. 1a) and

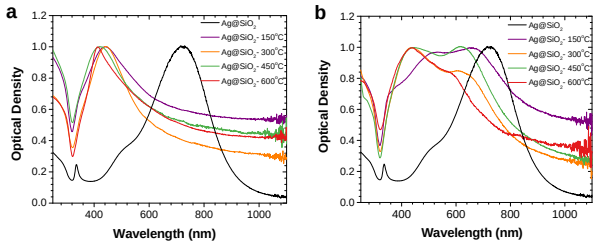

Fig. 1 Normalized UV-vis absorption spectra of Ag@SiO_2 nanotriangles after annealing in either an (a) air or (b) N_2 atmosphere.

N_2 (Fig. 1b). The plasmon bands of the Ag@SiO_2 nanotriangles that had been annealed in air were immediately and dramatically blue-shifted (λ_{LSPR} ≈ 420-440 nm) when compared to the as-synthesized nanotriangles (λ_{LSPR} ≈ 720 nm). The degree of blue-shifting was dependent on the annealing temperature, with the highest annealing temperature (600 °C) producing the most blue-shifted plasmon band (λ_{LSPR} ≈ 419 nm). In contrast, the samples annealed in N_2 showed a much more modest blue-shift upon annealing. The peak corresponding to the LSPR in-plane dipole mode blue-shifts from 720 nm to 660 nm upon annealing at 150 °C, and it blue-shifts further upon annealing at higher temperatures (615, 615, and 580 nm after annealing at 300, 450, and 600 °C, respectively). An additional peak at ca. 440 nm also appears in the spectra of all post-annealed samples. In the case of triangular nanoparticles, this gradual blue-shifting of the plasmon peak is generally attributed to a rounding of the particle tips and the resulting formation of nanodiscs; however, the distinct peak at *ca*. 420-440 nm is typical of spherical Ag nanoparticles. This suggests that the samples annealed in air are rapidly degraded into spherical byproducts, whereas the samples annealed in N_2 undergo a much more gradual morphology change.

In order to better understand these changes in particle morphology, we characterized the samples using TEM. Fig. 2 shows the TEM images of Ag@SiO_2 nanotriangles after annealing in air (Fig. 2a-d) and N_2 (Fig. 2e-h) atmospheres. The nanotriangles that were annealed in air at 150 °C showed the

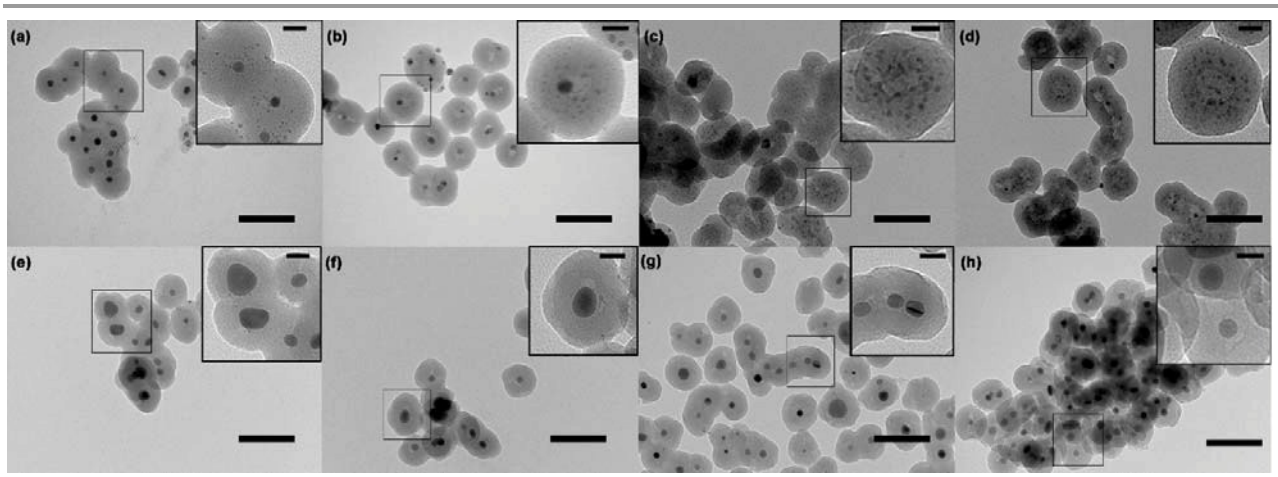

Fig. 2 TEM images of the Ag@SiO_2 nanotriangles after annealing in either (a-d) air, or (e-h) N_2 atmospheres. The samples were annealed at: (a,e) 150 °C, (b,f) 300 °C, (c,g) 450 °C, and (d,h) 600 °C. The scale bars in the main images are 100 nm, while those in the insets are 20 nm.

Dalton Transactions Accepted Manuscript

Please do not adjust margins

presence of round Ag core particles surrounded by a number of smaller nanoparticles embedded in the silica shell (Fig. 2a). Upon increasing the annealing temperature to 300 °C the Ag core shrunk further, in some cases leaving behind a hollow void in the silica shell. After annealing at either 150 or 300 °C, the Ag core was ca. 5 nm in diameter, and was surrounded by a large number of smaller particles (Fig. 2a and 2b inset). These larger Ag nanoparticles at the core of the SiO_2 shell are assumed to be the remnants of the original triangular Ag nanoparticles, while the smaller nanoparticles are formed from the material lost as the sharp tips decompose and fragment. After increasing the annealing temperature to 450 or 600 °C, the Ag cores completely disappeared. At these temperatures, the triangular core was completely fragmented into small Ag nanoparticles, leaving behind a hollow silica sphere (Fig. 2c-d). The size of these fragmented Ag nanoparticles was found to be relatively independent of temperature, with 450 °C (d = 2.5 ± 0.4 nm) and 600 °C (d = 2.3 ± 0.4 nm) producing similar sizes. These results are consistent with the UV-vis data presented previously; in all cases, only relatively small, spherical nanoparticles are observed, in agreement with the plasmon bands located at 420-440 nm. The larger cores observed in Fig. 2a and 2b would be expected to give rise to the plasmon bands at longer wavelengths (λ_{LSPR} ≈ 440 nm, Fig. 1a) than the smaller particles observed in Fig. 2c and 2d (λ_{LSPR} ≈ 420 nm, Fig. 1a).

The formation of hollow silica spheres has been observed previously by Lei *et al.* for spherical Ag@SiO_2 nanoparticles[37] and Kim *et al.*[44] for FeAuPd@SiO_2 nanoparticles after annealing the nanoparticles in air, which could be due to the diffusion of metal from the core. However, in neither of these cases did the central core fragment into smaller particles. In the present case, we hypothesize that the reason for the formation of such small Ag nanoparticles could be the size of the pores in SiO_2 around the Ag core.

In order to better understand this phenomenon, we synthesized Ag nanotriangles on a SiO_2 support (SiO_2@Ag) and annealed them at 450 °C and 600 °C. Fig. S2 shows the TEM images of the SiO_2@Ag nanoparticles after annealing. After annealing at 450 °C, spherical Ag nanoparticles were observed (Fig. S2b) and the size (11.0 ± 3.5 nm) of these nanoparticles was found to be much higher than for those formed upon Ag@SiO_2 annealing (Fig. 2c, d ~ 2.5 nm). Unlike the Ag@SiO_2 samples, for SiO_2@Ag there is no silica shell around the Ag nanotriangles to control the size of the particles formed after annealing. Upon increasing the annealing temperature to 600 °C, the SiO_2@Ag samples yielded smaller (7.5 ± 2.4 nm) nanoparticles (Fig. S2c). However, in both cases the Ag nanoparticles are still larger than those resulting from annealing of the Ag@SiO_2 samples. This indicates that, upon annealing the triangular Ag@SiO_2 core@shell nanoparticles, the silica shell restricts the ultimate size of the resulting Ag nanoparticles.

All of the samples annealed in a N_2 atmosphere showed the presence of residual Ag cores in the TEM images (Fig. 2e-h), regardless of annealing temperature. At low temperatures (150 °C), the core particle was only slightly rounded (Fig. 2e), in keeping with the modest blue-shift observed in the UV-vis spectrum (Fig. 1b). The degree of rounding is correlated with the annealing temperature, with the samples annealed at the highest temperatures having the smallest and roundest Ag cores. Again, this agrees with the more pronounced blue-shift of the plasmon bands observed in these samples (Fig. 1b). Unlike the samples annealed in air, no small particles were seen by TEM, indicating that the O_2 in the air is needed for the formation these small particles.

The thermal stability of the silver nanoparticles depends on the particle size and shape. Ag nanotriangles have a high aspect ratio, with (111) planes on the basal facets and either (110) or (100) planes on the edge facets.[30] As a result, the edges have a higher surface energy than the basal facets, hence they are less stable to corrosion. The vertices are even more unstable, since at vertices the two high energy edge facets intersect. Hence, upon annealing the Ag@SiO_2 nanotriangles, the decomposition process begins with the tips. In the presence of air, we hypothesize that the Ag core interacts with atmospheric oxygen and oxidizes to Ag_xO.[37, 45, 46] The atoms in the vertices are oxidized first; dissociation of the oxidized material leaves behind the circular nanoparticles observed in the cores of the SiO_2 particles (Fig. 2a-b). The smaller nanoparticles observed throughout the SiO_2 particle are then presumably composed of the dissociated material that was lost from the particle tips. Upon increasing the annealing temperature the Ag core further dissociates, leaving behind nothing but the smaller particles (Fig. 2c-d). In the presence of a N_2 atmosphere, since there is no possibility of Ag oxidation, we noticed a different change in the morphology of the Ag nanotriangles. This could be attributed to the migration of atoms from the tips (highly unstable features) to the more stable basal planes. The resulting morphology after migration is a particle with rounded tips and a similar overall size (Fig. 2e-f). This process becomes severe at higher annealing temperatures (Fig. 2g-h), which can lead to a complete rounding of the edges, and the deposition of a large number of atoms on the basal facets. This results in a pseudo-spherical nanoparticle, consistent with both the TEM images (Fig. 2g-h) and the LSPR band at ca. 420 nm (Fig. 1b). Such temperature dependent atomic migrations have been previously observed in modelling studies on Ag nanowires.[30]

Thermal degradation study of Ag@SiO_2 using XANES and EXAFS analysis

Since UV-vis spectroscopy and TEM provide no information on either the oxidation state or coordination environment of the resulting Ag@SiO_2 nanoparticles, we collected Ag *K*-edge X-ray absorption spectra. XANES (X-ray absorption near edge structure) spectroscopy is very specific to changes in valency, and EXAFS (extended X-ray absorption fine structure) is specific to the coordination environment of the absorbing metal atoms. The Ag *K*-edge spectra of all the samples were compared with reference spectra of Ag-foil and Ag_2O standards. The XANES spectra of Ag@SiO_2 nanotriangles before and after annealing in air and N_2 are shown in Fig. 3. Ag has a strong *K*-edge feature at 25514 eV which arises from dipole-allowed 2s to 5p transitions.

Dalton Transactions Accepted Manuscript

This journal is © The Royal Society of Chemistry 20xx

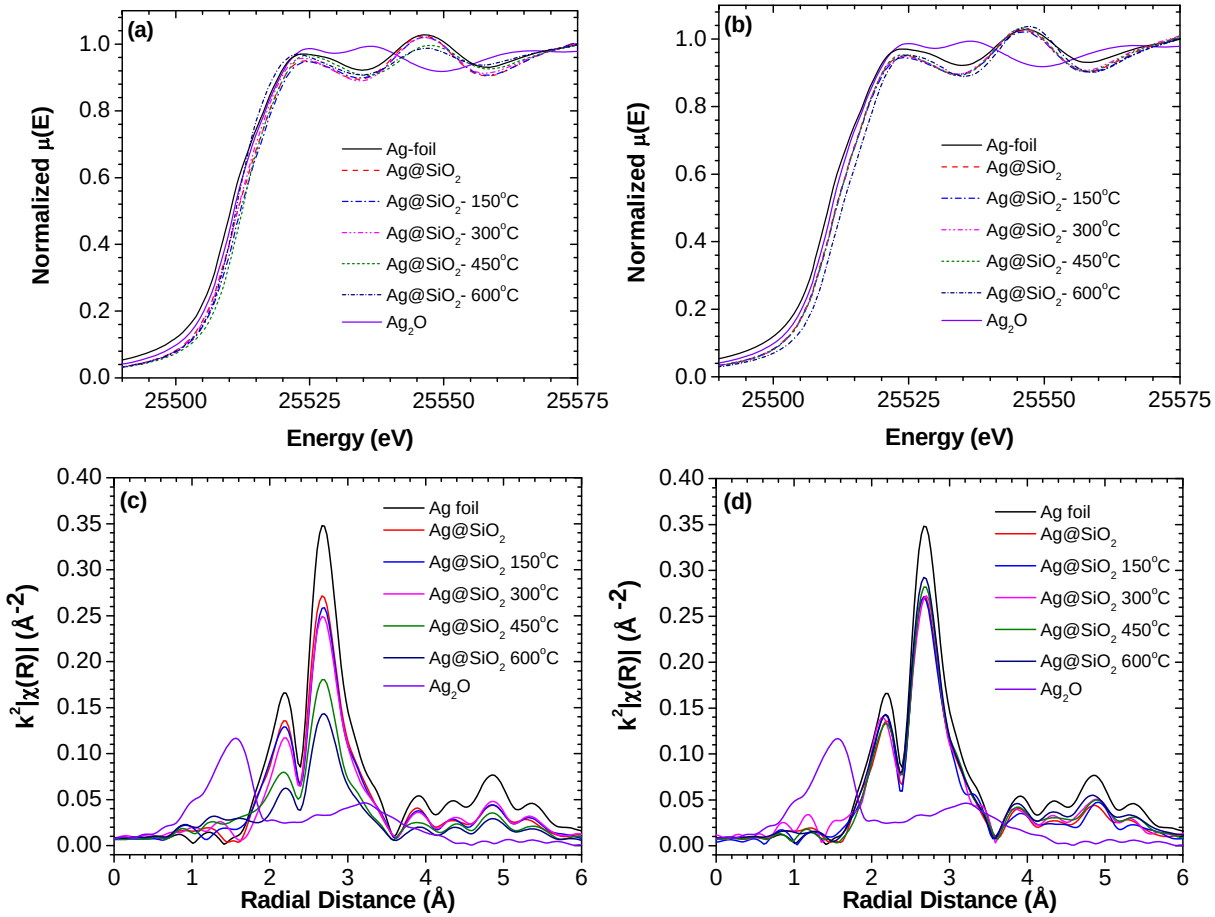

Fig. 3 Ag *K*-edge (a,b) XANES and (c,d) FT-EXAFS spectra of Ag@SiO_2 nanotriangles annealed in (a,c) air and (b,d) N_2. All spectra were collected at room temperature.

The near edge features of all samples were similar to those of the reference Ag-foil spectra. However, the samples annealed in air showed a decrease in the intensities of the near-edge peaks compared to the reference Ag-foil spectrum. This decrease in the intensity of these peaks with an increase in annealing temperature is due to a decrease in the size of the Ag nanoparticle (resulting in a lower overall coordination number for the Ag atoms). Such changes were not seen in the case of the Ag@SiO_2 samples annealed in N_2. Regardless of annealing atmosphere and temperature, none of the samples showed spectral features matching those of the Ag_2O reference, which indicates the presence of little-to-no Ag_2O in the annealed samples.

We also performed an EXAFS analysis to study the changes in Ag coordination environment upon annealing the Ag@SiO_2 nanoparticles. The EXAFS region is very sensitive to the bonding environment around the scattering atom. To study this, Ag *K*-edge spectra of all the samples annealed in air and N_2 were plotted as the Fourier-transformed radial distribution function (FT-EXAFS) and the first coordination shell of Ag was fit using a Ag fcc model. Fig. 3c and 3d show the experimental FT-EXAFS spectra of the Ag@SiO_2 samples in R space. All the samples showed peaks at 2.18 Å and 2.67 Å, which match well with the reference Ag foil spectra and are due to Ag-Ag first shell contributions. The Ag_2O bulk material standard spectra shows a major peak at 1.56 Å, which is due the first shell Ag-O contribution. Although the Ag@SiO_2 nanoparticles were annealed in air, none of the spectra have a peak at 1.56 Å, indicating a lack of oxidation in the annealed samples (i.e., they are almost completely Ag(0)). However, the intensity of the peak corresponding to the first shell Ag-Ag contribution decreases as the annealing temperature is increased from 150 °C to 600 °C in air. The intensity of this peak in the FT-EXAFS spectra is directly proportional to the Ag-Ag coordination number (note that the spectra are collected at room temperature after annealing). Hence, for the samples annealed in air, there is a decrease in the average Ag-Ag coordination number with increasing annealing temperature; this is directly correlated with a decrease in the size of the particles, as for smaller particles a higher percentage of Ag atoms are under-coordinated on the particle surface. The samples annealed in N_2 showed much more modest changes in the intensity of the Ag-Ag peak, indicating relatively little change in the overall particle size upon annealing in N_2. This is in agreement with the TEM

Dalton Transactions Accepted Manuscript

Please do not adjust margins

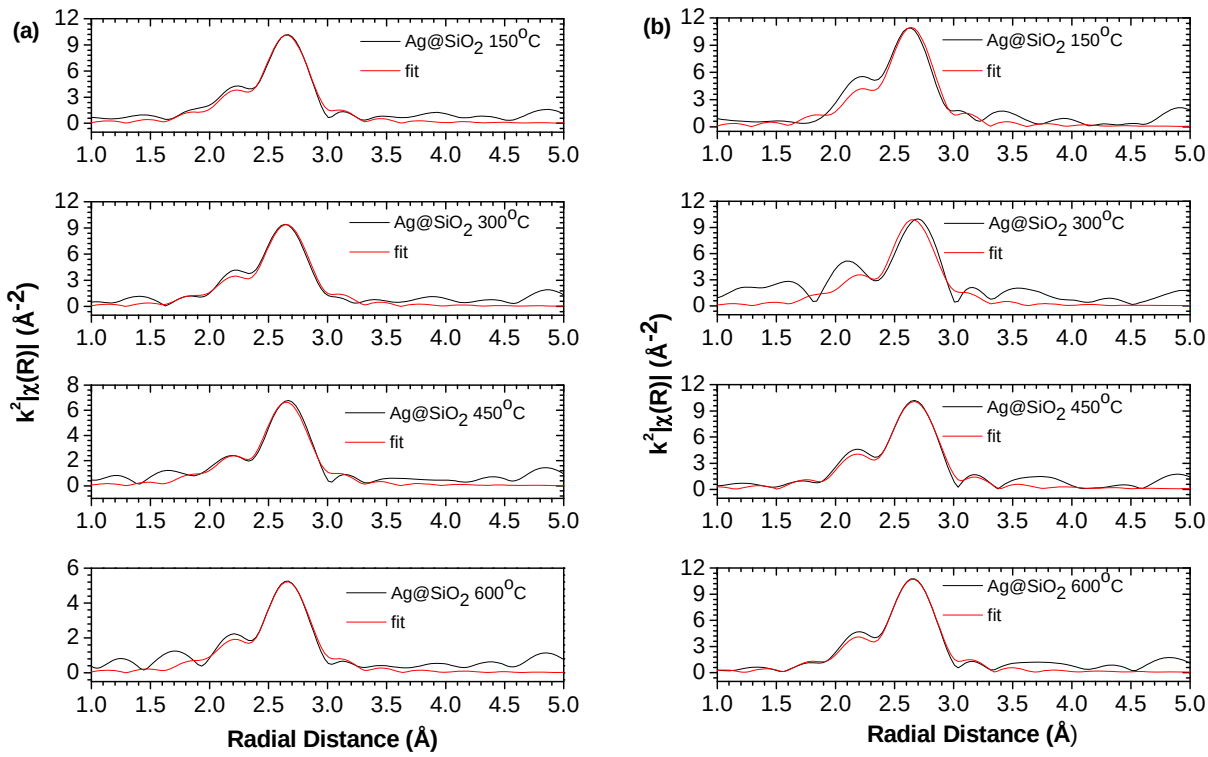

Fig. 4 EXAFS fitting of Ag@SiO_2 nanotriangles annealed in (a) air and (b) N_2 at different temperatures. All spectra were collected at room temperature after annealing.

Table. 1 EXAFS fitting parameters of Ag@SiO_2 nanotriangles annealed in air and N_2 at different temperatures, the amplitude factor for the fittings was kept at fixed value of 0.973

Ag@SiO_2 Annealing Temperature	Air				N_2			
	CN (Ag-Ag)	R/ Å (Ag-Ag)	σ^2/ Å^2	E_o (shift)/eV	CN (Ag-Ag)	R/ Å (Ag-Ag)	σ^2/Å^2	E_o (shift)/ eV
RT	10.3 (6)	2.855 (4)	0.0102 (6)	2.0 (3)	N/A	N/A	N/A	N/A
150 °C	9.0 (5)	2.860 (4)	0.0102 (5)	1.9 (3)	9.1 (4)	2.853 (6)	0.0098 (6)	1.3 (3)
300 °C	8.8 (5)	2.858 (4)	0.0105 (6)	1.5 (3)	10.2 (6)	2.860 (6)	0.0111 (9)	1.4 (4)
450 °C	6.6 (3)	2.861 (4)	0.0109 (5)	0.8 (3)	10.0 (6)	2.860 (5)	0.0106 (6)	1.5 (3)
600 °C	5.2 (4)	2.863 (6)	0.0108 (8)	1.7 (4)	10.5 (6)	2.861 (4)	0.0106 (6)	0.9 (3)

data, where the samples annealed at higher temperatures in air showed the presence of numerous small nanoparticles inside the silica sphere (Fig. 2a-d), whereas for the samples annealed in N_2, only larger particles at the core of the SiO_2 shell were observed (Fig. 2e-h).

To quantify these findings, EXAFS fitting was performed for all the samples using existing Ag crystallographic data (Fm-3m). Only the first shell single scattering path Ag_o-Ag_1 (R_{eff} = 2.88 Å, degeneracy = 12) was used as a model for fitting. The experimental EXAFS plot in R-space, along with the simulated EXAFS fitting of all the samples, is shown in Fig. 4 and the corresponding fitting parameters are tabulated in Table 1. A decrease in the 1st shell Ag-Ag coordination number with an increase in the annealing temperatures was observed for the samples annealed in air. This implies a decrease in the average size of the particles with an increase in annealing temperature, which is in agreement with the observed formation of small Ag nanoparticles (d ~ 3 nm) and complete loss of the central Ag core at higher annealing temperatures. Samples calcined at higher temperatures (450 °C, 600 °C) have low coordination numbers (6.6 and 5.2, respectively), indicating the presence of very small particles with a large number of surface atoms (< 2.5 nm). In the case of the samples annealed in N_2, only a small increase in the 1st shell Ag-Ag coordination number was observed, which is consistent with the migration of highly under-coordinated atoms from the tips of the triangles to the more stable basal planes, but an overall retention of the particle size.

This journal is © The Royal Society of Chemistry 20xx
Dalton Transactions Accepted Manuscript

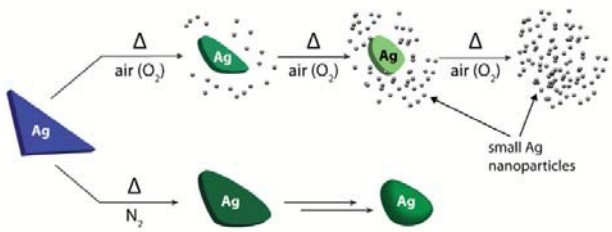

Fig. 5 Proposed thermal degradation mechanism of Ag nanotriangles in air and N_2. The silica shell is omitted for clarity.

It is known that Ag is prone to oxidation at elevated temperatures; however, from the EXAFS analysis there was no significant presence of Ag_xO after annealing in air. This indicates that any oxidation products must dissociate back to Ag and O_2. We postulate that upon annealing the Ag@SiO_2 nanotriangles in air, initially the vertices are oxidized to Ag_xO; this detaches from the triangle, leading to a rounding of the particle shape (Fig. 5). The dissociated Ag_xO then decomposes back into small Ag nanoparticles and O_2.[37, 47] This oxidation and dissociation process depends on both the annealing temperature and atmosphere. By TEM, it can be observed that these small Ag nanoparticles are spread throughout the silica sphere. The silver that is lost from the nanotriangle tips clearly diffuses inside the silica shell (either as Ag_xO or metallic Ag), but due to the thick silica shell, has difficulty reaching the particle surface. In the case of samples annealed in N_2, these small Ag nanoparticles were not seen; in the absence of any oxidation/dissociation process, the observed changes in particle morphology are most likely due to atomic migration from less stable surfaces to more stable basal planes. A simplified mechanism of this thermal decomposition process is shown in Fig. 5.

Conclusions

Using a combination of UV-vis spectroscopy, TEM and X-ray absorption spectroscopy, we have established a detailed mechanism for the thermal degradation of Ag@SiO_2 nanotriangles. Under all conditions studied, the triangular Ag@SiO_2 nanoparticles were found to be unstable, and displayed pronounced morphological changes. In the presence of air and at low annealing temperatures, truncation of the nanotriangles' tips was observed, and led to the formation of small nanoparticles surrounding the remaining Ag core. At higher temperatures the entire Ag core fragmented into these smaller nanoparticles. Our XANES and EXAFS analysis showed that these small particles are Ag(0), and provided further evidence of a decrease in particle size. The samples annealed in N_2 yielded truncated nanotriangles (rounded particles) without the formation of any small nanoparticles. This suggested that the Ag@SiO_2 samples annealed in air first oxidize to Ag_xO and subsequently decompose back to Ag(0). Understanding the mechanisms by which these unique nanomaterials degrade is the first step toward developing more stable compounds that could be exploited in a wide variety of plasmonic applications.

Acknowledgements

T. L. K. is a Canada Research Chair in Photovoltaics. This research was undertaken, in part, thanks to funding from the Canada Research Chairs program. The Natural Sciences and Engineering Research Council of Canada (NSERC) and the University of Saskatchewan are acknowledged for financial support. Ning Chen and Weifeng Chen are acknowledged for their assistance on XAS measurements. Ruwaid Rafiuddin and John Hayes are acknowledged for helpful discussions on XANES and EXAFS. XANES and EXAFS experiments described in this paper were performed at the Canadian Light Source, which is supported by the Natural Sciences and Engineering Research Council of Canada, the National Research Council Canada, the Canadian Institutes of Health Research, the Province of Saskatchewan, Western Economic Diversification Canada, and the University of Saskatchewan.

References

1. K. L. Kelly, E. Coronado, L. L. Zhao and G. C. Schatz, *J. Phys. Chem. C*, 2003, **107**, 668-677.
2. C. J. Murphy, T. K. Sau, A. M. Gole, C. J. Orendorff, J. Gao, L. Gou, S. E. Hunyadi and T. Li, *J. Phys. Chem. C*, 2005, **109**, 13857-13870.
3. E. Petryayeva and U. J. Krull, *Anal. Chim. Acta*, 2011, **706**, 8-24.
4. L. Lu, A. Kobayashi, K. Tawa and Y. Ozaki, *Chem. Mater.*, 2006, **18**, 4894-4901.
5. Y. C. Cao, R. Jin and C. A. Mirkin, *Science*, 2002, **297**, 1536-1540.
6. C. Gao , Z. Lu , Y. Liu , Q. Zhang, M. Chi, Q. Cheng and Y. Yin, *Angew. Chem., Int. Ed. Engl.*, 2012, **51**, 5629-5633.
7. E. Martinsson, M. M. Shahjamali, K. Enander, F. Boey, C. Xue, D. Aili and B. Liedberg, *J. Phys. Chem. C*, 2013, **117**, 23148-23154.
8. P. K. Jain, X. Huang, I. H. El-Sayed and M. A. El-Sayed, *Acc. Chem. Res.*, 2008, **41**, 1578-1586.
9. J. Sa, G. Tagliabue, P. Friedli, J. Szlachetko, M. H. Rittmann-Frank, F. G. Santomauro, C. J. Milne and H. Sigg, *Energy Environ. Sci.*, 2013, **6**, 3584-3588.
10. X. Zhou, G. Liu, J. Yu and W. Fan, *J. Mat. Chem.*, 2012, **22**, 21337-21354.
11. M. Murdoch, G. I. N. Waterhouse, M. A. Nadeem, J. B. Metson, M. A. Keane, R. F. Howe, J. Llorca and H. Idriss, *Nature Chem.*, 2011, **3**, 489-492.
12. Z. Bian, T. Tachikawa, P. Zhang, M. Fujitsuka and T. Majima, *J. Am. Chem. Soc.*, 2013, **136**, 458-465.
13. J. Zhang, Q. Xu, Z. Feng, M. Li and C. Li, *Angew. Chem., Int. Ed. Engl.*, 2008, **47**, 1766-1769.
14. T. Balcha, J. R. Strobl, C. Fowler, P. Dash and R. W. J. Scott, *ACS Catalysis*, 2011, **1**, 425-436.
15. M. K. Gangishetty, K. E. Lee, R. W. J. Scott and T. L. Kelly, *ACS Appl. Mater. Interfaces*, 2013, **5**, 11044-11051.
16. M. K. Gangishetty, R. W. J. Scott and T. L. Kelly, *Langmuir*, 2014, **30**, 14352-14359.
17. M. D. Brown, T. Suteewong, R. S. Kumar, V. D'Innocenzo, A. Petrozza, M. M. Lee, U. Wiesner and H. J. Snaith, *Nano Lett.*, 2011, **11**, 438-445.

Dalton Transactions Accepted Manuscript

Please do not adjust margins

18. H. A. Atwater and A. Polman, *Nature Mater.*, 2010, **9**, 205-213.
19. M. A. Green and S. Pillai, *Nature Photon.*, 2012, **6**, 130-132.
20. J. E. Millstone, G. S. Métraux and C. A. Mirkin, *Adv. Funct. Mater.*, 2006, **16**, 1209-1214.
21. K. Poorkazem, A. V. Hesketh and T. L. Kelly, *J. Phys. Chem. C*, 2014, **118**, 6398-6404.
22. A. P. Kulkarni, K. M. Noone, K. Munechika, S. R. Guyer and D. S. Ginger, *Nano Lett.*, 2010, **10**, 1501-1505.
23. M. M. Shahjamali, M. Salvador, M. Bosman, D. S. Ginger and C. Xue, *J. Phys. Chem. C*, 2014, **118**, 12459-12468.
24. K. E. Lee, A. V. Hesketh and T. L. Kelly, *Phys. Chem. Chem. Phys.*, 2014, **16**, 12407-12414.
25. B. Tang, S. Xu, J. An, B. Zhao, W. Xu and J. R. Lombardi, *Phys. Chem. Chem. Phys.*, 2009, **11**, 10286-10292.
26. L. Liu, C. A. Burnyeat, R. S. Lepsenyi, I. O. Nwabuko and T. L. Kelly, *Chem. Mater.*, 2013, **25**, 4206-4214.
27. Q. Zhang, J. Ge, T. Pham, J. Goebl, Y. Hu, Z. Lu and Y. Yin, *Angew. Chem., Int. Ed. Engl.*, 2009, **48**, 3516-3519.
28. B. Tang, S. Xu, X. Hou, J. Li, L. Sun, W. Xu and X. Wang, *ACS Appl. Mater. Interfaces*, 2013, **5**, 646-653.
29. B. Tang, J. An, X. Zheng, S. Xu, D. Li, J. Zhou, B. Zhao and W. Xu, *J. Phys. Chem. C*, 2008, **112**, 18361-18367.
30. E. Marzbanrad, G. Rivers, P. Peng, B. Zhao and N. Y. Zhou, *Phys. Chem. Chem. Phys.*, 2015, **17**, 315-324.
31. A. Volk, D. Knez, P. Thaler, A. W. Hauser, W. Grogger, F. Hofer and W. E. Ernst, *Phys. Chem. Chem. Phys.*, 2015, **17**, 24570-24575.
32. M. Á. Gracia-Pinilla, E. Pérez-Tijerina, J. A. García, C. Fernández-Navarro, A. Tlahuice-Flores, S. Mejía-Rosales, J. M. Montejano-Carrizales and M. José-Yacamán, *J. Phys. Chem. C*, 2008, **112**, 13492-13498.
33. Y. Yang, Q. Zhang, Z.-W. Fu and D. Qin, *ACS Appl. Mater. Interfaces*, 2014, **6**, 3750-3757.
34. C. Xue, X. Chen, S. J. Hurst and C. A. Mirkin, *Adv. Mater.*, 2007, **19**, 4071-4074.
35. P. Du, Y. Cao, D. Li, Z. Liu, X. Kong and Z. Sun, *RSC Advances*, 2013, **3**, 6016-6021.
36. D. Aherne, D. E. Charles, M. E. Brennan-Fournet, J. M. Kelly and Y. K. Gun'ko, *Langmuir*, 2009, **25**, 10165-10173.
37. Z. W. Lei, M. Liu, W. Ge, Z. P. Fu, K. Reinhardt, R. J. Knize and Y. Lu, *Appl. Phys. Lett.*, 2012, **101**, 083903.
38. Z. L. Wang, *J. Phys. Chem. C*, 2000, **104**, 1153-1175.
39. J. An, B. Tang, X. Zheng, J. Zhou, F. Dong, S. Xu, Y. Wang, B. Zhao and W. Xu, *J. Phys. Chem. C*, 2008, **112**, 15176-15182.
40. S. Chen, Z. Fan and D. L. Carroll, *J. Phys. Chem. C*, 2002, **106**, 10777-10781.
41. Q. Zhang, N. Li, J. Goebl, Z. Lu and Y. Yin, *J. Am. Chem. Soc.*, 2011, **133**, 18931-18939.
42. M. Newville, *J. Synchrotron Rad.*, 2001, **8**, 322-324.
43. B. Ravel and M. Newville, *J. Synchrotron Rad.*, 2005, **12**, 537-541.
44. Y. J. Kim, J. K. Choi, D.-G. Lee, K. Baek, S. H. Oh and I. S. Lee, *ACS Nano*, 2015, DOI: 10.1021/acsnano.1025b05860.
45. Q. Hua, A. Dimitri, G. Orest and S. M. Prokes, *Nanotechnology*, 2010, **21**, 215706.
46. M. Erol, Y. Han, S. K. Stanley, C. M. Stafford, H. Du and S. Sukhishvili, *J. Am. Chem. Soc.*, 2009, **131**, 7480-7481.
47. K. Chatterjee, S. Banerjee and D. Chakravorty, *Phys. Rev. B*, 2002, **66**, 085421.

Dalton Transactions Accepted Manuscript

This journal is © The Royal Society of Chemistry 20xx